Title

Liquefaction-induced softening of load transfer between pile groups and laterally spreading crusts

Journal

Journal of Geotechnical and Geoenvironmental Engineering, 133(1)

ISSN

1090-0241

Authors

Brandenberg, Scott J
Boulanger, R W
Kutter, Bruce L
et al.

Publication Date

2007

Peer reviewed

Liquefaction-Induced Softening of Load Transfer between Pile Groups and Laterally Spreading Crusts

Scott J. Brandenberg, A.M.ASCE[1]; Ross W. Boulanger, M.ASCE[2]; Bruce L. Kutter, M.ASCE[3]; and Dongdong Chang, S.M.ASCE[4]

Abstract: Laterally spreading nonliquefied crusts can exert large loads on pile foundations causing major damage to structures. While monotonic load tests of pile caps indicate that full passive resistance may be mobilized by displacements on the order of 1–7% of the pile cap height, dynamic centrifuge model tests show that much larger relative displacements may be required to mobilize the full passive load from a laterally spreading crust onto a pile group. The centrifuge models contained six-pile groups embedded in a gently sloping soil profile with a nonliquefied crust over liquefiable loose sand over dense sand. The nonliquefied crust layer spread downslope on top of the liquefied sand layer, and failed in the passive mode against the pile foundations. The dynamic trace of lateral load versus relative displacement between the "free-field" crust and pile cap is nonlinear and hysteretic, and depends on the cyclic mobility of the underlying liquefiable sand, ground motion characteristics, and cyclic degradation and cracking of the nonliquefied crust. Analytical models are derived to explain a mechanism by which liquefaction of the underlying sand layer causes the soil-to-pile-cap interaction stresses to be distributed through a larger zone of influence in the crust, thereby contributing to the softer load transfer behavior. The analytical models distinguish between structural loading and lateral spreading conditions. Load transfer relations obtained from the two analytical models reasonably envelope the responses observed in the centrifuge tests.

DOI: 10.1061/(ASCE)1090-0241(2007)133:1(91)

CE Database subject headings: Pile foundations; Pile groups; Earthquakes; Liquefaction; Lateral loads; Deformation; Solids; Softening.

Introduction

Loads from laterally spreading ground have been a major cause of damages to pile foundations in past earthquakes, particularly when a nonliquefied crust layer spreads laterally over underlying liquefied layers. For example, case histories after the 1995 Kobe earthquake (e.g., JGS 1996, 1998) showed that many piles that extended through a nonliquefiable crust layer, through a liquefiable layer, and down into competent soils were damaged near the top and bottom of the liquefied layer. Model studies have identified that loads from nonliquefied crust layers are often the critical loads that control the response of a pile foundation. For example, Dobry et al. (2003) found that the strength of the nonliquefied crust in analyses of their centrifuge tests significantly influenced pile bending moments, while subgrade reaction loads in the liquefied layer had a negligible effect on analysis results.

Lateral loads between pile foundations and nonliquefied crust layers are commonly represented as a function of the relative displacement between the pile foundation and the "free-field" ground (i.e., the ground displacement that would occur without any influence from the pile group) using a load transfer relation (the phrase "load transfer" will hereafter refer to lateral load versus relative displacement between the free-field crust and pile foundation). Load transfer behavior depends on how the stresses and strains induced by the pile group spread through the crust, thereby causing actual ground displacements to be different from "free-field" ground displacements (Fig. 1). Loading conditions during lateral spreading are fundamentally different from conditions in static load tests in nonliquefied ground, yet load transfer relations based on static tests (e.g., Rollins and Sparks 2002; Duncan and Mokwa 2001) are often applied to analyses of pile groups in lateral spreads because suitable relations for lateral spreading are not available. Brandenberg et al. (2005) showed that load transfer behavior during lateral spreading in centrifuge models was about an order of magnitude softer than load transfer relations from static field tests. The difference in load transfer relations was attributed to the effect of liquefaction on the stress distribution within the crust layer and on cyclic degradation and cracking in the crust materials.

This paper expands on the centrifuge data set in Brandenberg et al. (2005) by presenting analytical models for predicting load transfer between pile groups and laterally spreading crusts. A review of the centrifuge test program and observations of load transfer behavior are presented. Analytical models are then derived for two separate loading conditions in which: (1) the pile cap displaces into a stationary nonliquefied crust layer that over-

[1]Assistant Professor, Dept. of Civil and Environmental Engineering, Univ. of California at Los Angeles, Los Angeles, CA 90095-1593.

[2]Professor, Dept. of Civil and Environmental Engineering, Univ. of California at Davis, Davis, CA 95616-5294.

[3]Professor, Dept. of Civil and Environmental Engineering, Univ. of California at Davis, Davis, CA 95616-5294.

[4]Graduate Student, Dept. of Civil and Environmental Engineering, Univ. of California at Davis, Davis, CA 95616-5294.

Note. Discussion open until June 1, 2007. Separate discussions must be submitted for individual papers. To extend the closing date by one month, a written request must be filed with the ASCE Managing Editor. The manuscript for this paper was submitted for review and possible publication on September 27, 2005; approved on July 19, 2006. This paper is part of the ***Journal of Geotechnical and Geoenvironmental Engineering***, Vol. 133, No. 1, January 1, 2007. ©ASCE, ISSN 1090-0241/2007/1-91–103/$25.00.

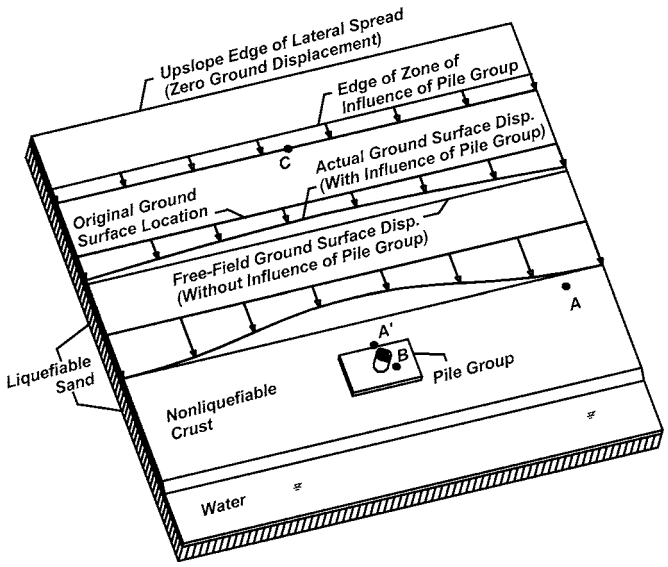

Fig. 1. Schematic of interaction between pile group and a laterally spreading nonliquefied crust

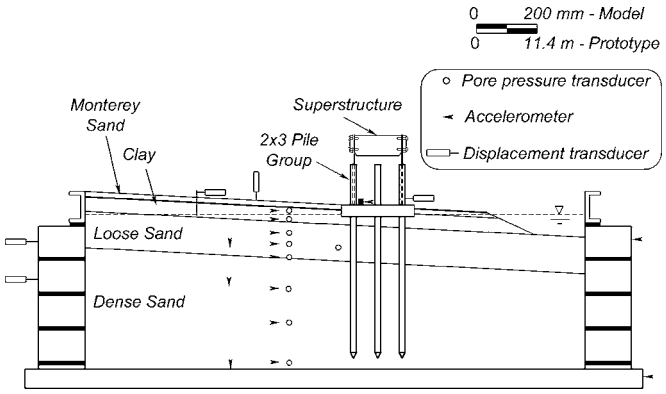

Fig. 2. Layout of Centrifuge Model DDC01 with most of the nearly 100 sensors omitted for clarity

lays liquefied soil, and (2) the nonliquefied crust layer spreads against a stationary pile cap. The analytical models provide a backbone curve intended to envelope the hysteretic dynamic response that occurs during earthquake shaking. Computed load transfer relations are compared with centrifuge observations. Limitations of the analytical models and the practical implications of these findings are discussed.

Centrifuge Tests

A series of dynamic centrifuge tests was performed on the 9-m radius centrifuge at the University of California at Davis, Davis, Calif. (Table 1). Details of the tests were presented by Brandenberg et al. (2005) and only an abbreviated summary is given herein. Fig. 2 shows the model layout for Centrifuge Test DDC01, which was similar to six other tests containing a six-pile group with a large embedded pile cap. The soil profile for all of the models consisted of a nonliquefiable clay crust overlying loose sand ($D_r \approx 21-35\%$) overlying dense sand ($D_r \approx 69-83\%$). All of the layers sloped gently toward a river channel carved in the crust at one end of the model. The sand layers beneath the crust were uniformly graded Nevada sand ($C_u=1.5$, $D_{50}=0.15$ mm).

Table 1. Soil and Pile Properties for Five of the Centrifuge Models

Test (ID)	Properties of six-pile group	Soil profile	N
PDS03	$b=0.73$ m, $I=4.5\times10^{-3}$ m^4 $L,W,H_{cap}=9.5,5.7,2.3$ m	4.2 m clay ($s_u=22$ kPa)[a] Over 4.6 m loose sand ($D_r\approx31\%$) Over dense sand ($D_r\approx79\%$)	38.1g
SJB01	$b=0.73$ m, $I=4.5\times10^{-3}$ m^4 $L,W,H_{cap}=10.1,6.5,2.5$ m	4.2 m clay ($s_u=44$ kPa)[a] Over 4.6 m loose sand ($D_r=33\%$) Over dense sand ($D_r=83\%$)	38.1g
SJB03	$b=1.17$ m, $I=24.0\times10^{-3}$ m^4 $L,W,H_{cap}=14.3,9.2,2.2$ m	1.4 m coarse sand Over 2.7 m clay ($s_u=44$ kPa)[a] Over 5.4 m loose sand ($D_r=35\%$) Over dense sand ($D_r=75\%$)	57.2g
DDC01	$b=1.17$ m, $I=24.0\times10^{-3}$ m^4 $L,W,H_{cap}=14.3,9.2,2.2$ m Superstructure $T=0.8$ s[b]	0.6 m coarse sand Over 3.6 m clay ($s_u=33$ kPa)[a] Over 5.4 m loose sand ($D_r=35\%$) Over dense sand ($D_r=75\%$)	57.2g
DDC02	$b=1.17$ m, I$=24.0\times10^{-3}$ m^4 $L,W,H_{cap}=14.3,9.2,2.2$ m Superstructure $T=0.3$ s[b]	0.6 m coarse sand Over 3.6 m clay ($s_u=22$ kPa)[a] Over 5.4 m loose sand ($D_r=35\%$) Over dense sand ($D_r=75\%$)	57.2g

Note: b=pile outer diameter; I=moment of inertia; L=pile cap length; W=pile cap width; H_{cap}=pile cap thickness; $E=68.9$ GPa; $\sigma_y=216$ MPa; and N=centrifugal acceleration.

[a]Average s_u value over layer thickness.

[b]Fixed-base natural period.

The nonliquefiable crust consisted of reconstituted bay mud (liquid limit ≈ 90, plasticity index ≈ 50) that was mechanically consolidated with a large hydraulic press, and subsequently carved to the desired slope. The average undrained shear strength of the crust, s_u, ranged from 22 to 44 kPa. A thin layer of coarse Monterey sand was placed on the surface of the bay mud for some of the models. Models were tested in a flexible shear beam container (FSB2) at centrifugal accelerations ranging from 38.1 to 57.2g. Water was used as a pore fluid. Results are presented in prototype units.

The pile diameters were 0.73 or 1.17 m (Table 1) spaced at four diameters center to center. The pile caps were embedded 2.2–2.5 m into the crust layer such that the upslope edge of the pile cap was flush with the ground surface. Single-degree-of-freedom structures with fixed-base natural periods of 0.8 and 0.3 s were connected to the pile cap for Tests DDC01 and DDC02, respectively.

Each test was shaken with a series of simulated earthquakes with sufficient time between shakes to allow dissipation of excess pore pressures. The simulated earthquakes were scaled versions of the acceleration recordings either from Port Island (83 m depth, north–south direction) during the Kobe earthquake, or from the University of California at Santa Cruz, Santa Cruz, Calif. (UCSC/Lick Laboratory, Channel 1) during the Loma Prieta earthquake. Generally, the shake sequence applied to the models was a small event ($a_{\max,\text{base}}=0.13-0.17g$) followed by a medium event ($a_{\max,\text{base}}=0.30-0.45g$) followed by one or more large events ($a_{\max,\text{base}}=0.67-1.00g$). Complete data reports from the centrifuge tests are available on the Center for Geotechnical Modeling website (http://nees.ucdavis.edu).

Measurements and Data Processing

Some forces and displacements were not directly measured, but rather were obtained by processing the raw recorded data. The techniques used to compute loads and relative displacements were explained in detail by Brandenberg et al. (2005) and Boulanger et al. (2003), and the aspects that are important for characterizing load transfer between pile groups and spreading crusts are briefly summarized herein.

Lateral Loads on Pile Caps

The lateral loads exerted on the pile groups by the crust layers were computed from measured pile shear forces and inertia loads based on the free-body diagram of horizontal forces in Fig. 3(a). The crust load, F_{crust}, contained contributions from passive force on the upslope face of the pile cap, friction forces along the sides and base of the cap, and loads on the pile segments beneath the cap, and was calculated from the recorded data using Eq. (1)

$$F_{\text{crust}} = (2V_s + 2V_n + 2V_c) - a_h \cdot m_{\text{cap}} - a_h \cdot m_{\text{structure}} \qquad (1)$$

where $-a_h \cdot m_{\text{cap}}$=cap inertia force; $-a_h \cdot m_{\text{structure}}$=superstructure inertia force; and V_s, V_c, and V_n=shear forces measured in the south, center, and north piles, respectively. Assuming symmetry, shear forces were measured in only three of the six piles (i.e., one of the south, center, and north piles), and were multiplied by 2 to account for the pile group being 2×3.

The value of $F_{\text{crust,ult}}$ can be controlled by two mechanisms: (a) the clay beneath the pile cap flows around the piles, thereby mobilizing lateral loads on the pile segments and friction loads at any contact between the crust and the base of the cap [Fig. 3(a)]; or

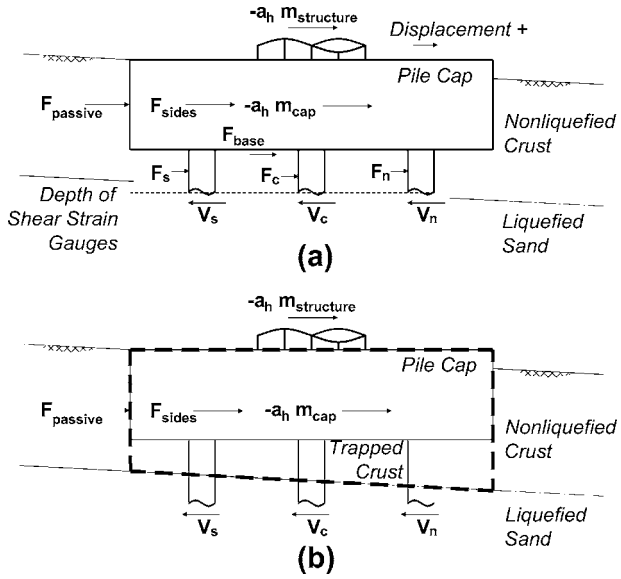

Fig. 3. Free-body diagram of horizontal forces acting on pile groups for mechanism in which (a) crust flows around piles; (b) crust becomes trapped between piles

(b) the clay crust beneath the pile cap becomes trapped between the piles, thereby acting as an equivalent block [Fig. 3(b)]. For Fig. 3(a), the contributions to $F_{\text{crust,ult}}$ are passive forces acting on the upslope face of the pile cap (F_{passive}), friction forces along the sides and base of the pile cap (F_{sides} and F_{base}, respectively), and forces on the pile segments beneath the crust (F_n, F_c, and F_s). For Fig. 3(b) the contributions to $F_{\text{crust,ult}}$ are passive forces acting on the upslope face of the equivalent block (i.e., along the full crust thickness) and friction forces between the sides of the equivalent block and laterally spreading crust. Lateral loads on the pile segments and friction along the base of the pile cap would be considered internal forces for the loading case in Fig. 3(b) (i.e., not external to a free body of the equivalent block). The controlling mechanism is that which produces the smaller total lateral load. The failure mechanism in Fig. 3(a), in which the clay crust flowed around the pile segments, was more appropriate for modeling loads on the piles in the centrifuge tests, as verified both by modes of soil deformation around the piles observed during excavation of the models (Brandenberg et al. 2004) and by comparison of theoretical predictions with measured loads (Brandenberg et al. 2005). Active forces on the downslope face of the cap were ignored due to the large gaps that formed along this face that remained open for the large earthquake motions.

Pile Cap and Crust Displacements

An overhead view of Centrifuge Model DDC01 after testing and after the surface layer of Monterey sand had been removed, thereby exposing the underlying clay, is shown in Fig. 4. The soil slopes downhill from the right side toward the left side of the photograph. Several grids of light-colored bentonite clay were placed on the surface of the darker bay mud during model construction to measure the displacement patterns caused by earthquake shaking. The original locations of the bentonite grid lines are shown in thin white lines and the locations after shaking are outlined in thicker white lines with fine lines connecting the before and after grids. The deformation patterns of the lines show that the large horizontal strains immediately upslope from the pile

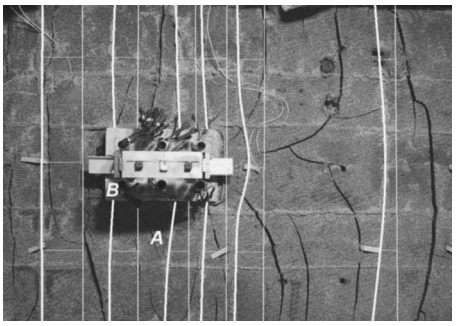

Fig. 4. Photograph of Model DDC01 off the centrifuge after testing with the surface of the bay mud exposed, and outlines of light-colored grid lines before and after shaking. The crust spread downslope from right to left in the photograph.

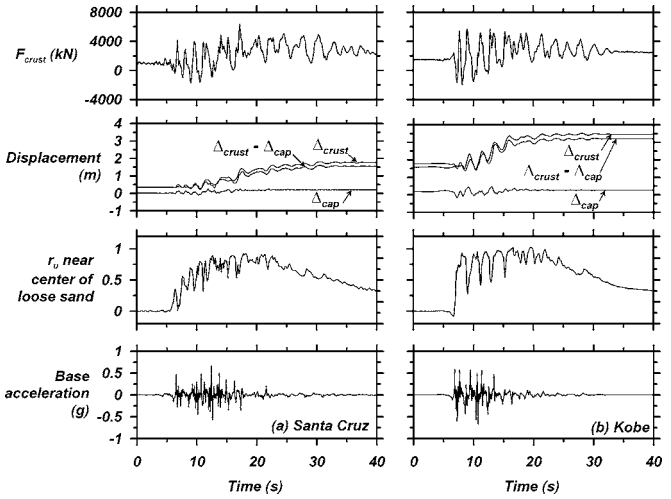

Fig. 5. Crust loads, pile cap and crust displacements, and excess pore pressure ratios for Test SJB03: (a) large Santa Cruz motion; (b) large Kobe motion

cap decrease gradually with distance and extend to a large distance upslope from the cap, which is evident in the curved bentonite grid line that was far upslope from the cap (far right in Fig. 4). The large zone of influence will later be shown to have a significant influence on the load transfer behavior.

Crust displacement and pile cap displacement (relative to the base of the container) were measured at Points A and B in Fig. 4, respectively. Time series of displacement were obtained by combining measurements from displacement transducers, anchored into the crust at Point A and attached to a pile at Point B, with transient displacements obtained by double-integrating filtered records from accelerometers embedded in the crust beneath Point A and attached to the pile cap. The displacement transducers provide accurate low-frequency response while the double-integrated acceleration records provide accurate high-frequency response, hence, combining the records with complementary filters (i.e., a low-pass filter on the displacement transducer and a high-pass filter on the double-integrated acceleration records, with the sum of the low-pass and high-pass filters equal to unity at all frequencies) can provide accurate displacements over a broad frequency band. A truly "free-field" displacement could not be recorded during the centrifuge tests because the pile groups influenced the crust displacements throughout the model, including some influence at Point A. The crust displacement recorded at Point A will be treated as a "free-field" displacement herein, and potential influences of this limitation will be discussed later.

Measured Load Transfer Behavior

Time series of crust load, displacement of the pile cap and crust, and excess pore pressure ratio (r_u) near the center of the loose sand layer are shown in Fig. 5 for the large Santa Cruz motion and large Kobe motion ($a_{max,base}=0.67g$ for both motions) for Model SJB03. The sequence of motions applied to the model was a small, medium, and large Santa Cruz motion, followed by a large Kobe motion. The small and medium motions caused nonzero initial crust loads and displacements evident at the beginning of the large Santa Cruz motion. Sufficient time was permitted between motions (i.e., more than 30 min) to allow pore pressures to dissipate. The ultimate crust load for this model, $F_{crust,ult}=6{,}380$ kN, was mobilized at about 17 s during the large Santa Cruz motion. The crust load during the subsequent large Kobe motion had several peak values ("peak" denotes a local maximum, while "ultimate" denotes the largest value during the shaking sequence) that were about 90% of $F_{crust,ult}$. Three observations indicate that $F_{crust,ult}$ was associated with mobilization of passive pressures in the crust: (1) relative displacement of the crust past the pile cap progressively accumulated during the shaking sequence, while the mobilized peak crust loads reached a plateau and did not continue to increase; (2) large concentrated shear strains were observed in the crust immediately upslope of the pile cap (see Fig. 4); and (3) back-calculated ultimate crust loads (Brandenberg et al. 2005) reasonably agreed with measured crust loads. The peak crust loads were slightly smaller during the Kobe motion than during the Santa Cruz motion, likely due to the cumulative effects of crack formation affecting the distribution of stresses in the crust (see Fig. 4), cyclic degradation in the crust's stress–strain behavior, and progressive loss of contact friction between the sides and base of the pile cap and the spreading crust.

For both motions, the crust loads reached their greatest values as the crust transiently lurched downslope during strong base shaking, and subsequently dropped to less than half of their peak values as ground displacements continued to increase after shaking. This is contrary to the common expectation that peak crust loads would be associated with the largest relative displacements between the pile cap and crust, and demonstrates that crust load depends on incremental, as well as total, relative displacements. Peaks in the crust loads coincided with transient reductions in the r_u values in the loose sand layer (i.e., from close to 1.0 to less than about 0.5). These reductions in r_u values are a consequence of the dilatancy of sand that is dense of its critical state (loose sand at low confinement in this case). As shear strains increase during undrained or partly drained loading, the dilatancy causes negative water pressures, thereby increasing effective stress, and increasing stiffness. During cyclic loading, the strain required to mobilize the dilatancy increases as the number of cycles increases. This class of behavior, observed in cyclic laboratory tests, was called "cyclic mobility" by Castro (1975). Cyclic mobility behavior has also been observed in cyclic $p-y$ relationships in liquefied sand (e.g., Wilson et al. 2000), and will be shown to also affect load transfer between pile groups and nonliquefied crusts.

Crust load is plotted versus relative displacement between the crust and pile cap in Fig. 6(a) for the large Santa Cruz motion for SJB03. The measured relation is much more complicated than the traditional concept of load transfer relations that characterize

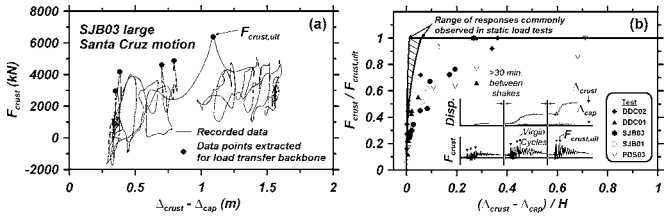

Fig. 6. (a) Recorded data for SJB03 for the large Santa Cruz motion; (b) backbone load transfer relations from five centrifuge tests

static load test behavior (e.g., Matlock 1970), whereby hysteresis loops track a characteristic backbone shape. For example, the loading cycle that mobilized $F_{\text{crust,ult}}$ is characterized by a displacement stiffening behavior in which tangent stiffness increases as crust load approaches $F_{\text{crust,ult}}$, and subsequently decreases as ground displacements continue to increase after $F_{\text{crust,ult}}$ is mobilized. This behavior may be partly attributed to cyclic mobility of the liquefied layer, whereby pore pressures in the liquefied sand layer transiently decrease causing the friction stresses imposed at the interface between the liquefied sand and crust to transiently increase. An increase in friction stresses along the base of the crust layer would be anticipated to have a stiffening effect on load transfer behavior based on the analytical models derived later in this paper. Other factors that probably influenced the load transfer behavior include ground cracking and gap formation in the crust, discontinuous movements of the blocks of crust material, cyclic degradation of the clay's stress–strain behavior, and loss of contact between the pile foundation and crust.

Backbone load transfer relations were developed by recording crust loads and relative displacements during virgin loading cycles in which the crust load exceeded the maximum past crust load for each test (Fig. 6). Ultimate crust loads, and pile group and soil layer geometries varied among the tests, so the crust loads for each test were normalized by $F_{\text{crust,ult}}$ recorded for that test, and the relative displacements were normalized by the thickness of the nonliquefiable crust (H) to facilitate comparison among the tests. Data extracted during virgin loading cycles show a characteristic backbone shape where crust load increases with increasing relative displacement, similar to a static $p-y$ relation. These backbone load transfer relations do not capture the complex hysteretic response observed during shaking, but are nevertheless useful for characterizing certain fundamental loading mechanisms that may reasonably envelope the dynamic response.

The load transfer data summarized in Fig. 6(b) for five tests show that $F_{\text{crust,ult}}$ values were mobilized at relative displacements ranging from about 25 to over 70% of the thickness of the nonliquefiable crust layer. For comparison, the load transfer behaviors from static load tests of pile groups and bulkheads (e.g., Rollins and Sparks 2002; Duncan and Mokwa 2001) are also summarized in Fig. 6(b), showing that passive pressures are mobilized at displacements equal to about 1–7% of wall height. The load transfer responses from the centrifuge test data were about an order of magnitude softer than observed in static load tests. The primary causes of the softer behavior are the influence of the underlying liquefiable sand on the distribution of stresses induced in the crust by the pile group, which is the focus of this paper, cracking and gap formation in the crust materials, and cyclic degradation of the clay's stress–strain behavior.

Load Transfer in a Crust over Liquefied Soil

The influence of underlying liquefiable sand on the soft load transfer behavior observed in the centrifuge tests was inadvertently explained by Terzaghi (1936) when he postulated that a uniform Rankine stress state can be attained throughout a soil deposit only if all boundaries are frictionless, including the boundary along the base of the deposit. Under plane strain loading conditions with such frictionless boundaries, the amount of displacement at one end of a deposit required to mobilize a Rankine failure state is proportional to its length rather than its height because displacement is equal to the integral of horizontal strains throughout the length of the deposit. Since a soil deposits' length is typically much larger than its height, a very soft load–displacement response would be expected. However, experience showed that passive pressures were mobilized at displacements proportional to wall height, not to deposit length, because friction along the base of the deposit caused stresses to be localized in a zone near the wall. A frictionless contact along the base of a deposit was perceived to be physically unrealistic, prompting Terzaghi to assert that Rankine stress states exist "only in our imaginations." Although Terzaghi's purpose was to demonstrate a limitation of Rankine earth pressure theory, it proved useful for explaining the soft load transfer behavior during lateral spreading in the centrifuge tests. Small friction stresses would be expected along on the base of a laterally spreading crust layer by underlying liquefied sand (i.e., when r_u is close to 1.0), which mimics the boundary conditions along the base of the deposit required for a Rankine stress state. Small friction stresses on the base of the deposit permit horizontal stresses and strains to geometrically spread within the crust to a large distance upslope from the foundation, far outside of the eventual failure wedge. The relative displacement required to mobilize passive pressures are, therefore, much larger when the crust is underlain by liquefied soil versus nonliquefied soil.

Derivation of Analytical Load Transfer Models

Analytical models for predicting load transfer behavior between a pile group and a nonliquefied crust overlying liquefied sand are presented in this section. The models represent the undrained strength of the liquefied sand layer as a constant residual strength (s_r), and account for different pile group and soil layer geometries, three-dimensional (3D) spreading of stresses in the crust, stress–strain behavior in the crust, and ground motion characteristics. Input parameters are described in Table 2. Models are derived for two simple conceptual cases wherein (1) the pile cap moves horizontally into a stationary soil mass (herein called the structural loading model), and (2) the nonliquefied crust layer spreads laterally toward a stationary pile group (herein called the lateral spreading model). The first might occur, for example, during a superstructure and/or pile cap inertia loading cycle when transient ground displacements are small, or during a static load test of a pile foundation in a soil profile that has been liquefied by blast charges (e.g., Ashford and Rollins 2002). The second might occur when laterally spreading soil fails in the passive mode and flows around a laterally stiff pile foundation that exhibits little cap displacement. Actual loading conditions would likely include some combination of ground displacement and pile cap displacement, and would, therefore, deviate from the loading conditions in the analytical models. The two simple loading cases are intended to merely envelope field loading behavior rather than to

Table 2. Input Parameters for Analytical Models

Parameter	Description	Baseline value
W	Pile cap width	10 m
H	Crust thickness	2.5 m
γ	Unit weight of crust material	16 kN/m^3
s_r	Residual strength of liquefied sand	4 kPa
s_u	Undrained shear strength of crust material	40 kPa
$F_{\text{crust,ult}}$	Ultimate lateral load exerted on pile group by crust	2,500 kN
α	Angle of attenuation of horizontal stresses in plan view	26.6 degrees
β	Angle of inclination of ground surface	3 degrees
F_{max}[a]	Small-strain horizontal stress-strain modulus	21,200 kPa
Motion[b]	Earthquake ground motion time history	Kobe

[a]Stress–strain relation defined by Vucetic and Dobry (1991) modulus reduction curve for PI=50.

[b]Lateral spreading model only.

capture every aspect of behavior. Furthermore, the analytical models cannot capture the hysteretic dynamic behavior that actually occurs during shaking [e.g., see Fig. 6(a)] because of their numerous simplifying assumptions (e.g., the undrained shear strength of liquefied sand transiently varies during shaking, but is represented as constant in the analytical models for simplicity). Despite these limitations, the models are useful for explaining certain aspects of measured behavior that had not previously been measured or anticipated, and they can be used to approximate more accurate load transfer relations for beam-on-springs-type design calculations.

Structural Loading Model

This section presents the derivation of the load transfer behavior for structural loading conditions in which the pile cap displaces into a stationary nonliquefied crust. The assumptions of the load transfer model are:

1. Inertia of the nonliquefied crust is neglected since the ground is assumed stationary (the influence of crust inertia is discussed later).
2. The residual strength of the liquefied sand is fully mobilized along the base of the nonliquefied crust and acts in the downslope direction against the force imposed by the pile group [Fig. 7(b)].
3. Stresses attenuate within a 3D block of stress influence that geometrically extends at an angle α from the backface of the pile cap in plan view [Fig. 7(d)].

While passive failure may be localized within a small region of crust near the pile cap, significant strains may extend further upslope into the crust, thereby affecting the relative displacements between the far-field crust and pile cap. Assuming stresses attenuate along an angle α is a mechanically simplified method analogous to the 2:1 rule that is commonly used to compute vertical stresses beneath a footing. Elastic solutions were considered in lieu of the simplified geometric attenuation model, but ultimately dismissed because the complexity of elastic solutions for the boundary conditions inherent to this problem is not justified by the simple treatment of other issues (e.g., the behavior of liquefied sand). The solution proceeds by first assuming an F_{crust} value, solving for strains induced within the zone of influence in the crust, and then integrating those strains to obtain relative displacement between the pile group and crust.

F_{crust} is the change in interaction force between the pile group and the crust layer during loading, so it is necessary to incorporate the initial interface horizontal stresses that existed prior to lateral loading into the model solution. The initial value of F_{crust} will be assumed equal to zero (i.e., at-rest pressures on the upslope side of the pile group are balanced by at-rest pressures on the downslope side), and the initial static shear stress on the base of the nonliquefied crust is solved by statics as $s_r+\gamma \cdot H \cdot \sin\beta$.

The change in lateral stress at some distance x upslope from the pile group can be solved by horizontal force equilibrium of a free body of the crust between the pile group and a plane cut perpendicular to the ground surface at x, as illustrated in Fig. 7. The change in force that must act on the plane to keep the free body in force equilibrium is defined by Eq. (2)

$$F(x) = F_{\text{crust}} - [s_r + \gamma \cdot H \cdot \sin\beta] \cdot [W \cdot x + x^2 \cdot \tan\alpha] \qquad (2)$$

At a distance x upslope from the pile group, the change in horizontal stress, $\Delta\sigma(x)$, is equal to $F(x)$ divided by the section area of the vertical plane in the stress block at x. Strain is equal to the stress divided by secant modulus, E', which may be a nonlinear function of strain, and is presented in the following equation:

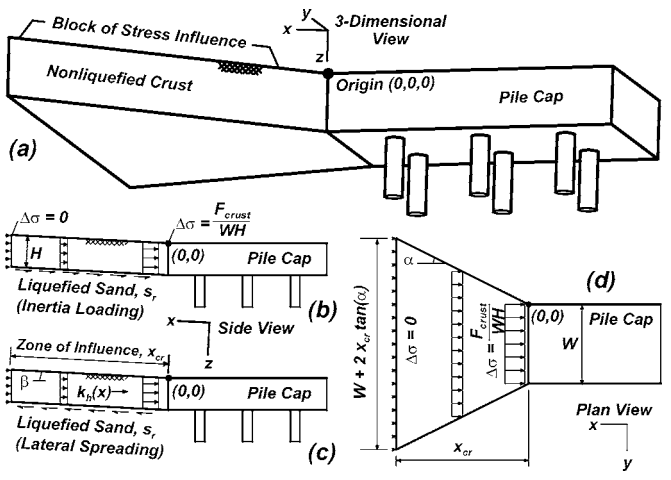

Fig. 7. Schematic of pile group and block of stress influence in nonliquefied crust behind pile group: (a) 3D view; (b) side view for structural loading model; (c) side view for lateral spreading model; and (d) plan view

$$\epsilon(x) = \frac{1}{E'}\left[\frac{F_{\text{crust}} - [s_r + \gamma \cdot H \cdot \sin\beta] \cdot [W \cdot x + x^2 \cdot \tan\alpha]}{H \cdot [W + 2 \cdot x \cdot \tan\alpha]}\right] \quad (3)$$

The x-direction secant modulus, E', is averaged over the thickness of the crust (H), and is analogous to, but not strictly equal to, the average Young's modulus (the constraining effect of out-of-plane stresses would cause E' to be larger than Young's modulus). The length of the zone of influence, defined as the location x_{cr} where change in horizontal stress is zero, can be found by setting $x=x_{cr}$ and $F(x_{cr})=0$, and subsequently solving Eq. (2) for x_{cr}. The positive part of the quadratic solution for x_{cr} is presented in the following equations:

$$x_{\text{cr}} = \frac{1}{2 \cdot C_1} \cdot [-C_2 + \sqrt{(C_2^2 + 4 \cdot C_1 \cdot F_{\text{crust}})}] \quad (4)$$

$$C_1 = [s_r + \gamma \cdot H \cdot \sin\beta] \cdot \tan\alpha \quad (5)$$

$$C_2 = [s_r + \gamma \cdot H \cdot \sin\beta] \cdot W \quad (6)$$

The relative displacement between the pile cap and the free-field nonliquefied crust (equal in magnitude to the pile cap displacement since the crust is assumed stationary) is equal to the integral of strain within the zone of influence as given in the following equation:

$$\Delta_{\text{rel}} = \int_0^{x_{\text{cr}}} \epsilon(x) \cdot dx \quad (7)$$

A closed-form solution for Δ_{rel} can be obtained by substituting the appropriate expressions for $\epsilon(x)$ and x_{cr}, provided that E' is constant. However, the resulting expression is too long to be practically useful and it is often desirable to assign the crust material a nonlinear stress–strain relationship in which secant modulus depends on strain. A discrete numerical integration approach was utilized in this paper, and required deriving equations for a single slice bounded between two planes perpendicular to the ground surface, one located at x_{i-1} (closer to the pile group) and the other at x_i. The expressions relating unknown force and strain on the upslope edge of a slice (F_i and ϵ_i, respectively) to known force and strain on the downslope edge (F_{i-1} and ϵ_{i-1}, respectively) are given in Eqs. (8) and (9)

$$F_i = F_{i-1} - [s_r + \gamma \cdot H \cdot \sin\beta] \cdot [W + (x_i + x_{i-1}) \cdot \tan\alpha] \cdot [x_i - x_{i-1}] \quad (8)$$

$$\epsilon_i = \frac{1}{E'} \cdot \frac{F_i}{H \cdot [W + 2 \cdot x_i \cdot \tan\alpha]} \quad (9)$$

The discrete numerical integration procedure is defined in the following steps:

1. Compute x_{cr} using Eqs. (4)–(6), and discretize the zone of influence into thin slices.
2. Beginning with the slice adjacent to the pile group, impose F_{crust} as a known force on the right edge of the slice.
3. Compute the strain on the right edge of the slice as $F_{crust}/(W \cdot H \cdot E')$.
4. Compute the force on the left edge of the slice using Eq. (8).
5. Compute the strain at the left edge of the slice using Eq. (9).
6. Impose the force on the left edge of the current slice as being equal and opposite to the force on the right edge of the next slice, and repeat Steps 4, 5, and 6 for all of the slices.
7. Compute the displacement by discretely summing strain × thickness of each slice.
8. Repeat Steps 2–7 for a sufficient number of different F_{crust} values to define the load transfer relation.

Lateral Spreading Model

This section presents the derivation of the load transfer behavior for lateral spreading conditions in which the nonliquefied crust spreads downslope against the stationary pile group. The assumptions of the load transfer model are:

1. Pile cap displacement is zero.
2. The residual strength of the liquefied sand is fully mobilized along the base of the nonliquefied crust and acts in the upslope direction to resist lateral spreading of the crust [Fig. 7(c)].
3. Stresses attenuate within a block of stress influence that geometrically extends at an angle α from the backface of the pile cap in plan view [Fig. 7(d)].
4. Horizontal acceleration and downslope displacement at a given location in the nonliquefied crust layer must be compatible with the acceleration versus displacement relation obtained from sliding block solutions (Newmark 1965) for a given ground motion (finding the compatible load transfer solution requires iteration).

The solution for the lateral spreading model follows the same logic as for the structural loading case, with the differences being the addition of crust inertia forces, and the change in direction of the shear stress from the liquefied sand layer. The change in stress along the bottom of the nonliquefied crust induced by the pile group is equal to $s_r - \gamma \cdot H \cdot \sin\beta$ since the initial static driving stress and the final residual stress act in the same direction.

The Newmark (1965) sliding block procedure provides a computationally simple method to capture the influence of ground motion on load transfer between pile groups and laterally spreading crusts. Applying the Newmark procedure to each slice of crust in the load transfer model is appropriate because each slice has its own unique yield acceleration defined as a function of the weight of the slice, the stress imposed on the bottom of the slice by the liquefied sand layer, and the difference in forces acting on the downslope and upslope edges of the slice. The lateral spreading load transfer model inherits all of the limitations of the Newmark procedure. For example: (1) the residual strength of the liquefied sand, which is known to vary during earthquake shaking (see Fig. 5), is assumed to be constant in the Newmark procedure; and (2) the influence of block deformations on sliding displacements is not accommodated by the rigid block assumption. The load transfer models are intended to be approachable design tools that approximate the principal aspects of behavior while maintaining a manageable level of computational complexity.

Stresses at some distance x upslope from the pile group can be solved by force equilibrium of a free body of the crust between the pile group and a plane cut perpendicular to the ground surface at x, as illustrated in Fig. 7. The change in force that must act on the plane to keep the slice in force equilibrium is defined in the following equation:

$$F(x) = F_{\text{crust}} + (s_r - \gamma \cdot H \cdot \sin\beta) \cdot [W \cdot x + x^2 \cdot \tan\alpha] - \int_0^x \gamma \cdot k_h(\xi) \cdot \cos\beta \cdot H \cdot (W + 2 \cdot \xi \cdot \tan\alpha) \cdot d\xi \quad (10)$$

where $k_h(x)$=horizontal acceleration in units of g, which is obtained by compatibility with Newmark sliding block analyses of a

ground motion; and ξ=dummy variable used for evaluating the integral. A closed-form solution for $F(x)$ cannot easily be obtained for the lateral spreading model because (a) $k_h(x)$ is a nonlinear function of block displacement (as defined by the Newmark solution) and (b) block displacement is a function of slice forces. An incremental procedure was adopted herein, which required modifying Eq. (10) such that it relates an unknown force on the upslope side of a discrete element (F_i) to a known force on the downslope side (F_{i-1}), as given in Eq. (11)

$$F_i = F_{i-1} + (s_r - \gamma \cdot H \cdot \sin\beta) \cdot [W + (x_i + x_{i-1}) \cdot \tan\alpha] \cdot (x_i - x_{i-1}) - \gamma \cdot k_h(x_{i-1}) \cdot \cos\beta \cdot H \cdot [W + (x_i + x_{i-1}) \cdot \tan\alpha] \cdot (x_i - x_{i-1}) \quad (11)$$

The solution is carried out in the following steps:

1. Define a relation between yield acceleration and sliding displacement using the Newmark (1965) sliding block procedure for a given ground motion and soil profile.
2. Select a length of the zone of influence and discretize the crust inside the zone of influence into thin slices.
3. Beginning with the slice adjacent to the pile group, select a trial value of F_{crust} (iteration will be required to obtain the solution).
4. Compute the strain in the slice at the contact with the pile group as $F_{crust}/(W \cdot H \cdot E')$.
5. Obtain the k_h value for the slice from the Newmark sliding block results based on the displacement of the right side of the slice (zero displacement for the first slice).
6. Compute the force on the left edge of the slice using Eq. (11).
7. Compute the strain at the left edge of the slice using Eq. (9).
8. Compute the displacement of the left edge of the slice as the strain at the right edge of the slice × slice thickness plus displacement on the right edge of the slice.
9. Set the force on the left edge of the current slice equal and opposite to the force on the right edge of the next slice and repeat Steps 5–9 for all of the slices.
10. Check if the force on the left edge of the last slice is reasonably close to zero, and if it is not, repeat Steps 3–10 until it is.
11. Repeat Steps 1–10 for a sufficient number of different ground motions (or scaled versions of a single motion) to define the load transfer relation.

The length of the zone of influence selected in Step 2 depends on the boundary conditions, and might be geometrically limited to the anticipated landward extent of lateral spreading (e.g., see Tokimatsu and Asaka 1998). In cases where the length of spreading soil is not limited by a boundary condition, x_{cr} should be sufficiently large that the solution becomes insensitive to further increases in x_{cr}. Each ground motion will give a single combination of crust load (F_{crust}) and relative displacement (displacement at the left edge of the last slice). To define the entire load transfer relation, the procedure must be repeated for a number of different ground motions, or scaled versions of a single motion.

Example Solutions of Analytical Load Transfer Models

The analytical models for structural loading and lateral spreading conditions are used to compute load transfer relations for a baseline set of parameters (Table 2) that are in the range of values from the centrifuge model tests (see Table 2). For the lateral spreading model, the input motions included a Kobe ground motion (baseline case), a Santa Cruz motion, and sinusoidal motions with five and 40 uniform 2 Hz cycles. The Newmark solutions for these motions are shown in Fig. 8 (k_{max}=maximum horizontal acceleration; k_y=yield acceleration; and Δ_{crust}=crust displacement). The ultimate crust load ($F_{crust,ult}$) was computed using Rankine passive earth pressure theory as $F_{crust,ult} = 1/2 \cdot \gamma \cdot K_p \cdot H^2 \cdot W + 2 \cdot s_u \cdot H \cdot W$, where K_p=1.0 for undrained loading (i.e., for ϕ=0). The stress–strain relation used for the crust layer fits the backbone curve for Vucetic and Dobry's (1991) modulus reduction curve for clay with PI=50, and $E'_{max} = 530 \cdot s_u$, which resulted in the ultimate stress being mobilized at 20% horizontal strain.

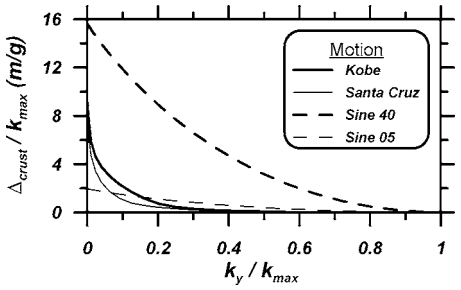

Fig. 8. Newmark sliding block solutions of sliding displacement versus yield acceleration

Distributions of Displacement and Stress

Distributions of relative displacement and stress versus distance from the pile cap for the baseline case are shown in Fig. 9 for $F_{crust}=F_{crust,ult}$. The relative displacement between the pile cap and the free-field soil surface (at x_{cr}) was 0.38 m for the structural loading model (x_{cr}=20 m) and 0.56 m for the lateral spreading model ($x_{cr} \approx 100$ m). Soil stresses extended further upslope to a larger zone of influence for the lateral spreading model than for the structural loading model, which reflects fundamental differences in the two load transfer models. For the structural loading model, the liquefied sand resists the horizontal soil stresses induced by the pile cap. For the lateral spreading model the stresses

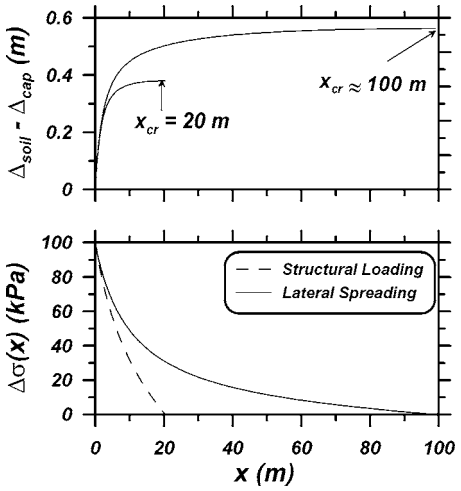

Fig. 9. Distributions of soil/pile group relative displacement and horizontal stress from baseline case solutions

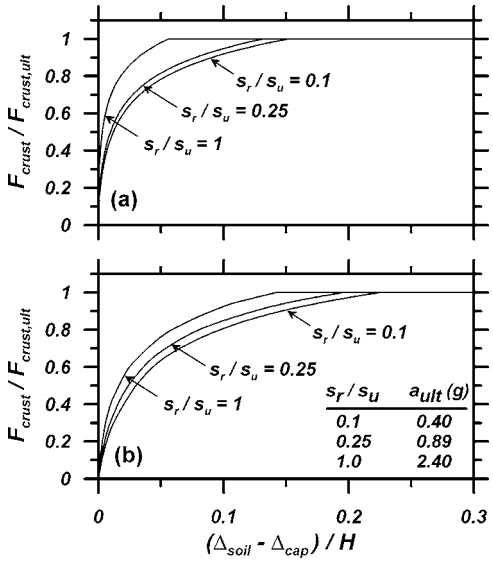

Fig. 10. Influence of ratio of residual strength (s_r) to crust undrained shear strength (s_u) on load transfer relation for (a) structural loading; (b) lateral spreading

from the liquefied sand and the stresses induced by the pile cap both act upslope on each crust block, and are balanced by the downslope crust inertia forces. The distributions of stress and displacement in the crust layer depend on the mechanical properties of the crust, the strength of the liquefied sand layer, and the angle of stress attenuation for both models, and also depend on ground motion characteristics for the lateral spreading model. The distributions for the baseline case are, therefore, specific to the input parameters in Table 2, and are not general characteristics of the analytical models.

Influence of Residual Strength of Liquefied Sand

The influence of the residual strength (s_r) of the liquefied sand layer on the computed load transfer relations is presented in Fig. 10, where s_r is expressed as a fraction of the crust layer's undrained shear strength (s_u). The curve for $s_r/s_u=0.1$ is for the baseline case, with the other curves corresponding to increasing s_r/s_u. As s_r/s_u increases, the load transfer relation stiffens for both models because, as expected, an increase in shear stress on the base of the nonliquefied crust layer is associated with a stiffening load–displacement response. The load transfer curves were softer for the lateral spreading model than for the structural loading model because of the larger zone of influence (Fig. 9) required to achieve equilibrium. For the structural loading model with $s_r/s_u=1.0$, the ultimate lateral load is mobilized at a relative displacement of 6% of the crust thickness (Table 3). These loading conditions are similar to static load testing of a pile foundation in a uniform deposit of nonliquefied crust material, and the computed load transfer curve is comparable to that observed in static load tests of pile caps (e.g., Rollins and Sparks 2002). The peak ground acceleration required to mobilize $F_{crust,ult}$ (which will be referred to as a_{ult}) for the lateral spreading model increased significantly as s_r increased (inset of Fig. 10). $F_{crust,ult}$ was mobilized at $a_{ult}=0.4g$ for $s_r/s_u=0.1$ (baseline case), and at $a_{ult}=2.4g$ for $s_r/s_u=1.0$. This is consistent with the observation that high s_r values have associated large yield accelerations that must be overcome to compress the spreading crust layer against the pile group.

Table 3. Summary of Influence of Parameters Variations on Load Transfer Results

	Structural loading model	Lateral spreading model	
Paramerer variation	$(\Delta_{rel}/H)_{ult}$[a]	$(\Delta_{rel}/H)_{ult}$[a]	a_{ult} (g)[b]
Baseline	0.15	0.29	0.40
$s_r/s_u=0.25$	0.11	0.20	0.89
$s_r/s_u=1.0$	0.06	0.15	2.40
$W/H=1.0$	0.05	0.08	0.25
$W/H=10.0$	0.32	0.50	0.63
$\alpha=0°$	0.56	0.63	0.63
$\alpha=45°$	0.09	0.18	0.79

[a]Normalized relative displacement at the first point where $F_{crust}=F_{crust,ult}$.

[b]Peak ground acceleration required to mobilize $F_{crust,ult}$.

Influence of Pile Cap Width

The influence of pile cap width on the computed load transfer relations is presented in Fig. 11 for width-to-height ratios of $W/H=1$, 4 (baseline case), and 10. As W/H increases, the displacement required to mobilize the peak load increases for both models because the length of the zone of influence increases with increasing pile cap width. The a_{ult} values for the lateral spreading model also increase because larger accelerations are required to compress the soil within the larger zone of influence. For the Kobe motion, $a_{ult}=0.25g$ for $W/H=1$, while $a_{ult}=0.63g$ for $W/H=10$. Compared with the influence of residual strength of the liquefied sand layer, pile cap width more significantly influenced the shape of the load transfer relations, but less significantly influenced a_{ult}.

Influence of Angle of Stress Attenuation

The influence of the angle of stress attenuation, α, on load transfer behavior is presented in Fig. 12 for $\alpha=0$, $\alpha=26.6°$ (2:1, baseline case), and $\alpha=45°$ (1:1). The load transfer relations become

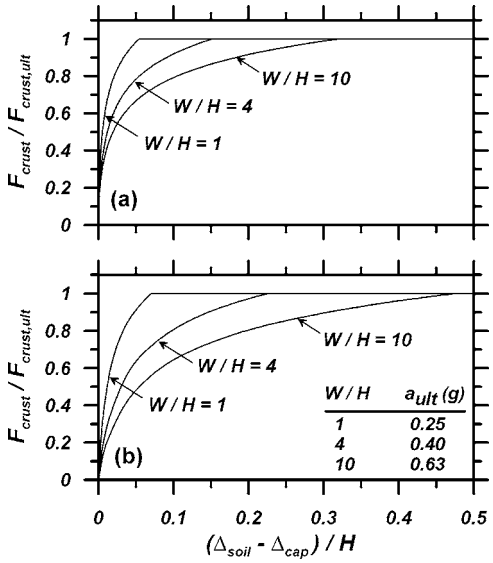

Fig. 11. Influence of ratio of pile cap width to layer thickness on load transfer relation for (a) structural loading; (b) lateral spreading

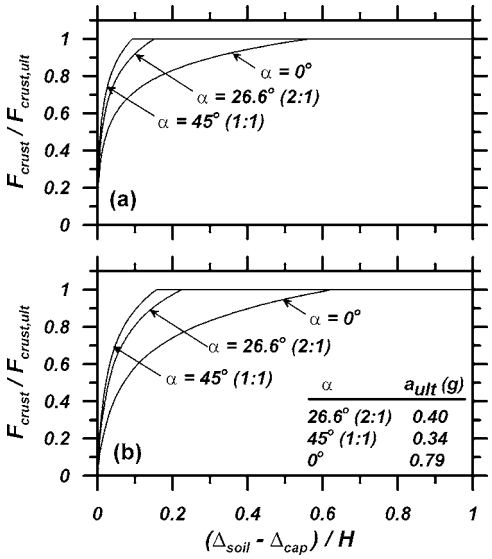

Fig. 12. Influence of angle of out-of-plane stress spreading on load transfer relation for (a) structural loading; (b) lateral spreading

stiffer as α increases because the more rapid attenuation of stresses causes the length of the zone of influence to decrease. For the case with $\alpha=0°$, stresses attenuate within a prismatic stress block and the load transfer relation is very soft. The accelerations required to mobilize $F_{\text{crust,ult}}$ for the lateral spreading model increase with decreasing α because large a_{ult} values are required to mobilize the requisite ground displacements.

Influence of Ground Motion

The influence of the ground motion on the lateral spreading analytical model is presented in Fig. 13 for the Kobe motion (baseline case), Santa Cruz motion, and sine wave motions of five and 40 uniform 2 Hz cycles (Fig. 13, Sine 05 and Sine 40, respectively). The computed load transfer curves are nearly identical for all four motions, but the a_{ult} values vary considerably. $F_{\text{crust,ult}}$ is reached at $a_{\text{ult}}=0.40g$ for the Kobe motion (baseline case), $0.54g$ for the Santa Cruz motion, $0.38g$ for the Sine 05 motion, and $0.18g$ for the Sine 40 motion. Comparing the Sine 40 and Sine 05 motions demonstrates how duration affects the a_{ult} values, and comparing the Kobe and Santa Cruz motion demonstrates the influence of frequency content on a_{ult} since these motions had nearly the same duration.

The fact that the shape of the computed load transfer relation is essentially independent of ground motion characteristics is an

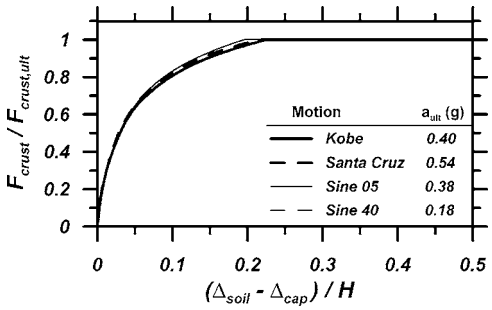

Fig. 13. Influence of ground motion on analytical load transfer model for lateral spreading conditions

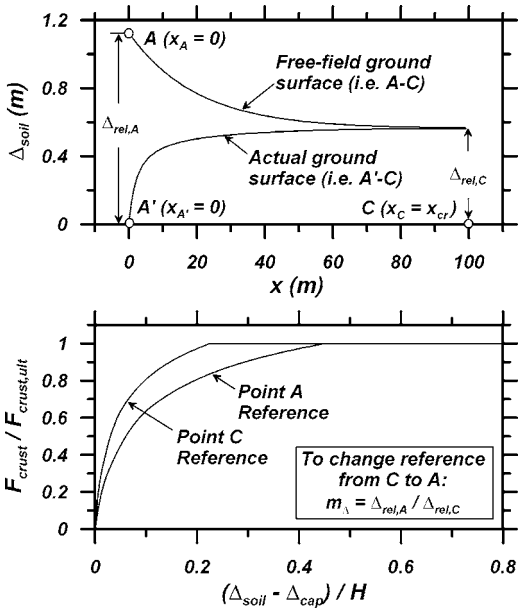

Fig. 14. Influence of point of reference within lateral spread on load transfer relation (see Fig. 1 for location of Points A, A′, and C)

artifact of the analytical model's underlying assumptions. The actual dynamic trace of lateral load versus relative displacement during earthquake shaking, shown in Fig. 6(a), suggests that the load transfer relation is affected by cyclic mobility behavior of the underlying liquefied soil, cyclic degradation of the crust materials, cracking of the crust layer, and possibly other factors. These factors depend on the duration, amplitude, and frequency content of the ground motion, hence, their influence on load transfer behavior would be expected to depend on ground motion as well. The analytical model does not directly account for such factors, and this is why the computed load transfer relation does not properly reflect its likely dependence on ground motion characteristics.

Correction for Point of Reference within Lateral Spread

A stiffness correction may be applied to the load transfer curves for the lateral spreading model to change the point of reference within the lateral spread. For lateral spreading toward an open face, displacements are largest at the face and decrease with distance landward (e.g., Tokimatsu and Asaka 1998) due to extensional strains and ground cracking. The derived analytical load transfer curves relate F_{crust} with displacement between the pile cap and the soil surface at a distance x_{cr} upslope from the pile cap (i.e., between Points B and C in Fig. 1). However, the traditional approach is to relate F_{crust} to the free-field soil displacement that would occur at the pile group location in the absence of any influence from the pile group (i.e., between Points A and C in Fig. 1). The effect of these alternative points of reference is illustrated in Fig. 14, which shows how ground displacements would vary with upslope position immediately behind the pile group (i.e., between Points A′ and C), and also for the free-field case far away from the pile group (i.e., between Points A and C). Plane strain deformations are assumed such that the free-field displacement at Point A is the same as the free-field displacement at Point A′. The ground surface displacement increases from zero immediately upslope of the pile group (Point A′, $x_{A'}=0$) to a value of

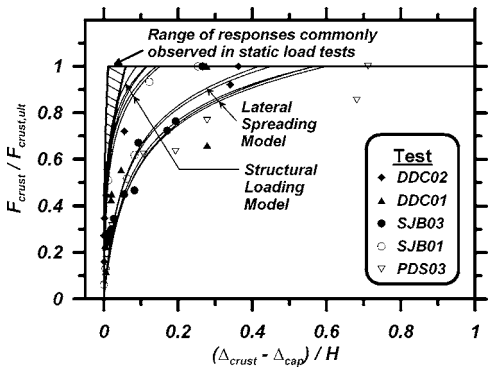

Fig. 15. Load transfer behavior measured in centrifuge tests compared with behavior predicted by structural loading model and lateral spreading model

0.56 m at the upslope limit of the zone of influence (Point C; x_C=100 m). The free-field ground surface displacement is also equal to 0.56 m at Point C because ground displacements at this point are not influenced by the pile group. However, in the absence of pile restraining forces, ground displacements increase with distance downslope toward the pile group location, becoming 1.12 m at x=0 at Point A. The relative displacement between the pile cap and the soil at the upslope extent of the zone of influence (between Points B and C) is $\Delta_{rel,C}$=0.56 m, while the relative displacement between the pile cap and the free-field soil at the pile group's location (between Points B and A) is $\Delta_{rel,A}$ =1.12 m. Hence, a correction to the load transfer relation is required to shift the point of reference from Point C (point of reference in the load transfer model) to Point A (conventional point of reference). In this case, a relative displacement multiplier of 2 is required ($m_\Delta=\Delta_{rel,A}/\Delta_{rel,C}=2$) to appropriately soften the load transfer relation. Note that the ground is stationary for the structural loading analytical model, so no correction for reference point is necessary.

There are some additional complicating mechanisms that must be considered when defining the load transfer relation relative to the free-field Point A. For free-field conditions, lateral spreading is accompanied by ground cracking that largely accounts for the variation in ground surface displacements with distance from the free face. In the centrifuge experiments, this means that the measurement of dynamic load transfer relations between Points A and B shown on the photograph in Fig. 4 is complicated by the hysteretic behavior of ground cracks, which are highly nonlinear and dependent on factors that are ill defined (e.g., infilling of cracks with sand ejecta). The analytical model for lateral spreading does not explicitly account for ground cracking, but rather can only attempt to approximate its influence through appropriate parameter selections and the relative displacement multiplier approach illustrated in Fig. 14.

Comparisons with Centrifuge Data

The load transfer data from five centrifuge tests are compared in Fig. 15 to the computed structural loading and lateral spreading load transfer relations for the Kobe base motion for each test. The baseline input parameters from Table 2 were used along with undrained shear strength, crust thickness, and ground surface slope from Table 1. Relative displacement values predicted by the lateral spreading model were multiplied by 2 to account for the ground displacements being measured at the pile group location rather than further upslope at the edge of the zone of influence (i.e., at Point A in Fig. 4). This multiplier was based on measurements of crust displacements near the pile cap location compared with displacements further upslope, and is consistent with the analysis presented in the previous section. The structural loading model captures the stiffer observed data points, while the lateral spreading model more closely fits the softer data points. Some of the data points are softer than the predicted range, which could be caused by uncertainty in the analytical model parameters (e.g., s_r; α; stress–strain relation for the crust) or the basic limitations of the analytical models (e.g., omission of cyclic degradation effects; soil–container interaction; vertical motions caused by container rocking; non-free-field movement at the location where crust displacements were measured). Nevertheless, the two analytical load transfer relations much more closely match the centrifuge test results than the "rule of thumb" behavior derived from static load tests.

The large zones of influence predicted by the analytical models are consistent with the observed deformation patterns in the clay crusts in the centrifuge model tests. For example, the photograph in Fig. 4 suggests that the stresses from the pile cap caused crust deformations near the end of the model container about 50 m upslope in prototype dimensions, which is consistent with the structural loading and lateral spreading analytical models predicting x_{cr}=20 and 100 m, respectively, for the representative baseline case. The container likely influenced the load transfer behavior in the centrifuge by impeding the progression of the zone of influence to even larger distances upslope.

Discussion

Backbone load transfer relations relative to a free-field crust displacement, as extracted from virgin loading cycles in the centrifuge tests, were an order of magnitude softer than static loading relations, but it is difficult to ascertain just how general this experimental observation is. Crust load versus relative displacement between the pile cap and free-field spreading crust, as observed in the centrifuge tests, showed a complex hysteretic response that depended on cyclic mobility behavior of the underlying liquefied sand, cyclic degradation of the crust materials, and the effects of ground cracking on the relative displacements between the pile cap and the free-field reference point. Dilatancy of the liquefiable sand layer was particularly apparent in the recorded load transfer behavior, and this interaction warrants further studies for clarification since it was not addressed in this paper. The observed behavior is likely affected by test variables (e.g., ground motion characteristics, soil profile, pile group configuration), and experimental limitations (e.g., soil–container interaction effects), which cannot be isolated using the available experimental data.

The analytical load transfer models for structural loading and lateral spreading were developed for two purposes: (1) to explain the influence of underlying liquefied sand on the softening of the load transfer relation in the crust, and (2) to evaluate how different variables affect the computed load transfer relations, and therefore assist in understanding how the observed relation might be extended to other conditions. The analytical models showed that the effect of liquefaction on the stress distribution in the crust layer contributed significantly to the softening of the load transfer behavior observed in the centrifuge tests. Additional softening in the centrifuge test data was caused by cyclic degradation of the crust material and cracking of the crust, which are only indirectly accounted for in the analytical load transfer models by the appro-

priate choice of strain-dependent moduli and by shifting the point of reference using a relative displacement multiplier. Finite-element analyses could potentially account for these additional effects, but also have a limited ability to capture ground cracking, gapping at foundation-to-soil interfaces, and lateral spreading displacement distributions. Considering the complications involved, the analytical load transfer models do provide insight into some of the fundamental mechanisms and provide a rational basis for estimating behavior for pile and soil conditions beyond those studied herein.

The softer load transfer relations observed in the centrifuge tests and computed in the analytical models (as opposed to the stiffer load transfer behavior observed in field and laboratory tests on nonliquefied, monotonically loaded retaining walls and pile caps) may affect design practice in different ways depending on the design approach and anticipated loading conditions. For example, a beneficial reduction in lateral load may be predicted when lateral spreading displacements are small (i.e., tens of centimeters), which might occur when the liquefiable layer is moderately dense or for small-to-medium ground motions, as shown in Brandenberg (2005). However, if lateral spreading displacements are large enough to mobilize $F_{crust,ult}$, then the mobilized crust load will not depend on the shape and stiffness of the load transfer relations, only their capacity. Alternatively, for structural loading conditions (i.e., inertia forces from the superstructure and/or pile cap), pile cap displacements could be underpredicted using load transfer relations based on static tests in nonliquefied soil. Larger-than-expected pile cap displacements caused by softer-than-expected load transfer behavior could result in poorer performance of the foundation and structure. For dynamic problems, it is often impossible to determine a priori which are the critical loading conditions, and a range of different possibilities that encompasses the various sources of uncertainty (e.g., in the load transfer relations, inertia forces, free-field ground displacements) should be considered to envelop the potential field responses.

Summary and Conclusions

The lateral load transfer behavior between laterally spreading nonliquefied crusts and pile groups was characterized by centrifuge tests and analytical models. Backbone relations for the hysteretic dynamic load transfer responses between the pile groups and the free-field nonliquefied crust, as observed in the centrifuge tests, were developed from the virgin peaks in the dynamic crust loads. The backbone relations were about an order of magnitude softer than the relations that have been obtained from static load tests in nonliquefied ground. The softening of the load transfer behavior can be beneficial for sites where moderate lateral spreading displacements do not fully mobilize passive pressure against the pile foundation, and detrimental for sites where large structural inertia forces cause larger-than-anticipated pile cap displacements.

The focus of this paper was the mechanism by which liquefaction of an underlying sand layer causes soil-to-pile-group interaction stresses to be distributed through a large zone of influence in the crust, thereby contributing to softer load transfer behavior. Analytical models accounted for the undrained shear strength of the liquefied layer (represented as a constant residual strength), the geometry of the pile group and spreading crust, spatial attenuation of horizontal soil-to-pile-group interaction stresses, nonlinear stress–strain behavior in the crust layer, ground motion characteristics, and the point of reference on the nonliquefied crust that is used for computing relative displacements. The influence of cyclic degradation and cracking within the nonliquefied crust was only approximately addressed. Analytical models were developed for structural loading conditions, in which the pile cap displaces into a stationary soil mass, and for lateral spreading conditions, in which the nonliquefied crust layer displaces toward a stationary pile group. Relations obtained from the two analytical models, with reasonable variations in the input parameters, provided an approximate envelope of the responses observed in the centrifuge tests. Considering the complexity of soil–structure interaction mechanisms during liquefaction-induced lateral spreading, the analytical load transfer models provide a reasonable and tractable basis for estimating the load transfer behavior for pile and soil conditions beyond those studied herein.

Acknowledgments

Funding was provided by the Pacific Earthquake Engineering Research (PEER) Center, through the Lifeline Program and the Earthquake Engineering Research Centers Program of the National Science Foundation, under Contract No. 2312001. The centrifuge tests were funded by Caltrans under Contract Nos. 59A0162 and 59A0392. The contents of this paper do not necessarily represent a policy of either agency or endorsement by the state or federal government. Recent upgrades to the centrifuge have been funded by NSF Award No. CMS-0086566 through the George E. Brown, Jr., Network for Earthquake Engineering Simulation (NEES). The writers appreciate the assistance of Dr. Dan Wilson with the centrifuge tests and data analysis techniques.

References

Ashford, S. A., and Rollins, K. M. (2002). "TILT: The Treasure Island liquefaction test: Final report." *Rep. No. SSRP-2001/17*, Dept. of Structural Engineering, Univ. of California at San Diego, San Diego.

Boulanger, R. W., Kutter, B. L., Brandenberg, S. J., Singh, P., and Chang, D. (2003). "Pile foundations in liquefied and laterally spreading ground during earthquakes: Centrifuge experiments and analyses." *Rep. UCD/CGM-03/01*, Center for Geotechnical Modeling, Univ. of California at Davis, Davis, Calif., ⟨http://nees.ucdavis.edu⟩.

Brandenberg, S. J. (2005). "Behavior of pile foundations in laterally spreading ground." Ph.D. dissertation, Univ. of California at Davis, Davis, Calif.

Brandenberg, S. J., Boulanger, R. W., Kutter, B. L., and Chang, D. (2005). "Behavior of pile foundations in laterally spreading ground during centrifuge tests." *J. Geotech. Geoenviron. Eng.*, 131(11), 1378–1391.

Brandenberg, S. J., Boulanger, R. W., Kutter, B. L., Wilson, D. W., and Chang, D. (2004). "Load transfer between pile groups and laterally spreading ground during earthquakes." *Proc., 13th World Conf. on Earthquake Engineering*, Paper 1516, Vancouver, Canada.

Castro, G. (1975). "Liquefaction and cyclic mobility of saturated sands." *J. Geotech. Engrg. Div.*, 101(6), 551–569

Dobry, R., Abdoun, T., O'Rourke, T. D., and Goh, S. H. (2003). "Single piles in lateral spreads: Field bending moment evaluation." *J. Geotech. Geoenviron. Eng.*, 129(10), 879–889.

Duncan, M. J., and Mokwa, R. L. (2001). "Passive earth pressures: Theories and tests." *J. Geotech. Geoenviron. Eng.*, 127(3), 248–257.

Japanese Geotechnical Society (JGS). (1996). "Special issue on geotechnical aspects of the January 17, 1995, Hyogoken-Nambu earthquake." *Soils Found.*, 1(SI1), 1–359.

Japanese Geotechnical Society (JGS). (1998). "Special issue on geotechnical aspects of the January 17, 1995, Hyogoken-Nambu earthquake." *Soils Found.*, 1(SI2), 1–209.

Matlock, H. (1970). "Correlations of design of laterally loaded piles in soft clay." *Proc., Offshore Technology Conf., Houston*, 577–594.

Newmark, N. M. (1965). "Effects of earthquakes on dams and embankments." *Geotechnique*, 15(2), 139–160.

Rollins, K. M., and Sparks, A. (2002). "Lateral resistance of full-scale pile cap with gravel backfill." *J. Geotech. Geoenviron. Eng.*, 128(9), 711–723.

Terzaghi, K. (1936). "A fundamental fallacy in earth pressure computations." *J. Boston Soc. Civ. Eng.*, 23, 71–88.

Tokimatsu, K., and Asaka, Y. (1998). "Effects of liquefaction-induced ground displacements on pile performance in the 1995 Hyogoken-Nambu earthquake." *Soils Found.*, 1(SI2), 163–177.

Vucetic, M., and Dobry, R. (1991). "Effect of soil plasticity on cyclic response," *J. Geotech. Engrg.*, 117(1), 89–107.

Wilson, D. W., Boulanger, R. W., and Kutter, B. L. (2000). "Observed seismic lateral resistance of liquefying sand." *J. Geotech. Geoenviron. Eng.*, 126(10), 898–906.